
EventPrune: Cascaded Event-Assisted Token Pruning for Efficient First-Person Dynamic Spatial Reasoning

Pengtao Ma^{1,†}, Ziliang Zhou^{1,†}, Ciyu Ruan¹, Haoyang Wang¹, Kaiyuan Li¹,
Zihang Gong², Wenhua Ding¹, Chen Gao³, Jingao Xu⁴, Xinlei Chen¹

¹Shenzhen International Graduate School, Tsinghua University, ²Harbin Institute of Technology,
³Tsinghua University, ⁴The University of Hong Kong

Abstract

First-person dynamic spatial reasoning requires models to track continuous motion and precise geometric structure, but the quadratic attention cost of Transformer-based Video-LLMs makes dense visual tokens computationally expensive. Existing token pruning paradigms predominantly rely on discrete static snapshots, failing to preserve the motion and geometric cues essential for reasoning. We propose Event Cascade Pruning (ECP), to our knowledge the first training-free framework that leverages the high-frequency motion cues from event cameras as a continuous event-guided motion prior to guide token selection. ECP combines three stages: Event-Triggered Causal Sampling to anchor motion-informative keyframes, Event-guided Motion Saliency Filtering to suppress event-inactive visual tokens, and Event-Attention Ranking Fusion to calibrate spatial attention with motion-salient dynamics. With 80% visual token reduction, ECP outperforms the full-token baseline (37.62% vs. 36.31%) while achieving $1.89\times$ inference speedup and 52% GFLOPs reduction. We further introduce ESR-Real, the first real-world RGB-event benchmark for first-person spatial reasoning, where ECP improves accuracy by 2.68 percentage points over full-token baselines.

1 Introduction

Video-LLMs [19, 31, 5] are increasingly used for first-person dynamic spatial reasoning [42, 33, 12], such as indoor navigation and drone perception [44, 30, 14]. Unlike conventional video understanding, embodied scenarios involve rapid egocentric motion and continuously changing scene geometry [6, 32]. These settings require models to process video efficiently [17, 38] while preserving motion continuity and geometric structures for reliable spatial reasoning.

To mitigate the “visual token explosion” and high inference latency in these real-time settings, training-free visual token pruning has become an important optimization strategy [9, 41, 17]. However, existing RGB-only pruning signals are fragile for highly dynamic egocentric videos at both temporal and spatial levels. (1) For inter-frame pruning, existing methods filter temporal redundancy by comparing pixel differences or feature similarities [43]. Such appearance-based comparison not only introduces significant latency but also fails to capture continuous dynamic characteristics like speed and trajectory, making it unreliable for dynamic information extraction. (2) For intra-frame pruning, methods based on attention weights [9, 23, 41] or diversity metrics [3, 21] may discard structure-critical tokens. Our analysis reveals a severe peripheral spatial bias in attention scores: attention concentrates disproportionately on image borders (Fig. 3), causing task-relevant interior regions to be under-retained. Diversity- or merging-based strategies may scatter retained tokens or merge local neighborhoods, fragmenting object boundaries and weakening geometric continuity.

[†]Equal contribution.

Consequently, existing pruning methods often fail to preserve the motion and structural cues required for spatial reasoning under high compression.

In contrast to existing software-based approaches, we identify event cameras as a natural external cue for these issues. As bio-inspired sensors that asynchronously record pixel-level brightness changes with microsecond resolution, event cameras offer unique cues for both dynamics and geometry: (1) At the inter-frame level, event streams directly record motion activity at each pixel. This provides an instant, training-free prior for anchoring causally critical transitions and filtering temporally redundant regions without expensive feature matching. (2) At the intra-frame level, events exhibit high sensitivity to edges and textures, representing the geometric structures that biased attention mechanisms neglect. These signals offer a reliable reference to calibrate attention scores and ensure the retention of tokens with true spatial saliency.

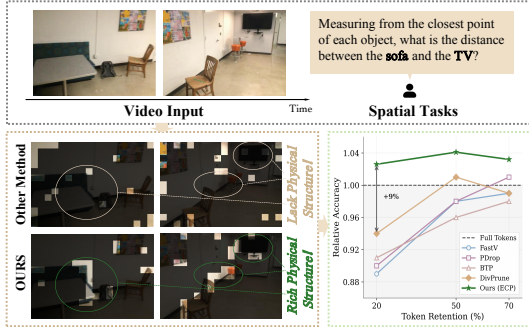


Figure 1: Token pruning for spatial reasoning. Unlike prior pruning, ECP preserves task-relevant geometric cues under high sparsity.

However, events are asynchronous external signals, fundamentally heterogeneous from the synchronous grid features inside Video-LLMs. How to deeply integrate this heterogeneous prior into the inference pipeline to genuinely guide token selection remains non-trivial. To overcome this, we propose Event Cascade Pruning (ECP), a training-free event-assisted pruning framework with three cascaded modules. Event-Triggered Causal Sampling (ETCS) anchors keyframes using event activity flux and temporal changes; Event-guided Motion Saliency Filtering (EMSF) removes low-motion regions via event saliency maps; and Event-Attention Ranking Fusion (EARF) calibrates attention-based token scores through non-parametric rank alignment, preserving tokens with joint event-semantic saliency.

Extensive experiments demonstrate the effectiveness of ECP. At 20% token retention, ECP outperforms all evaluated training-free pruning baselines and surpasses the full-token baseline (37.62% vs. 36.31%), while achieving $1.89\times$ speedup and 52% GFLOPs reduction. On our real-world ESR-Real benchmark with native event signals, ECP improves over the full-token baseline by 2.68 points at 50% retention. These results show that event-assisted pruning improves efficiency while preserving, and in some cases improving, accuracy for first-person dynamic spatial reasoning.

Our main contributions are:

- (1) We propose Event Cascade Pruning (ECP), to our knowledge the first training-free event-assisted pruning framework for first-person dynamic spatial reasoning, establishing a cascaded temporal-spatial-representation pruning pipeline that removes redundancy while preserving motion, geometric, and attention-derived semantic cues.
- (2) We introduce ESR-Real, a real-world RGB-event benchmark for first-person spatial reasoning with over 700 QA pairs across 6 categories.
- (3) We achieve the best performance among evaluated training-free pruning methods: ECP outperforms the full-token baseline at 80% token reduction with $1.89\times$ speedup and 52% GFLOPs reduction, with consistent gains on both simulated-event and real-event benchmarks.

2 Related Work

Video-LLMs and First-Person Dynamic Spatial Perception. Recent Large Vision-Language Models (LVLMs) [2, 20, 24, 4, 37, 11] integrate visual encoders with LLMs [34, 1] for unified multimodal understanding. Representative Video-LLMs such as LLaVA-NeXT [25], Qwen2.5-VL [5], and LLaVA-OneVision [19] improve fine-grained and long-context video understanding, but their high-resolution visual tokens lead to substantial computational cost. This bottleneck is especially problematic for first-person dynamic spatial reasoning, where models must respond to rapid ego-motion and changing geometry under latency constraints.

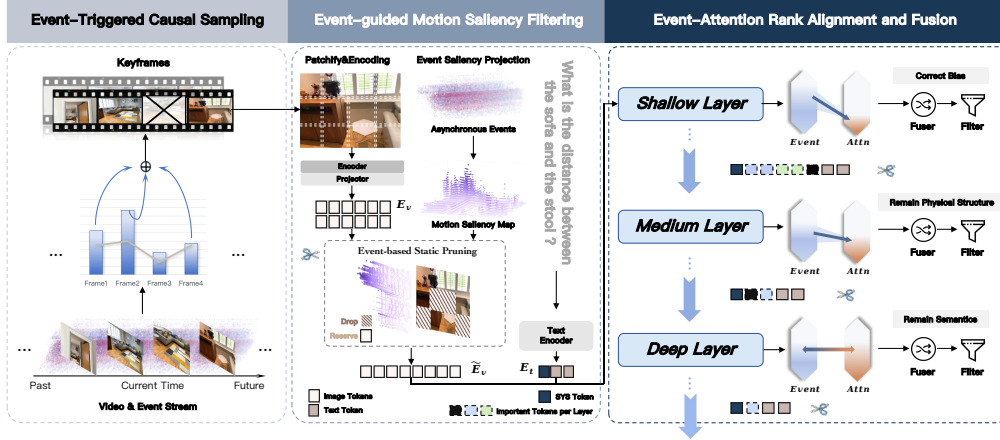


Figure 2: Overview of Event Cascade Pruning (ECP). ECP comprises three cascaded modules: ETCS selects keyframes via event activity flux; EMSF prunes static regions using motion saliency maps; EARF calibrates attention with event priors, applying layer-wise fusion weights.

Visual Token Pruning. To mitigate computational bottlenecks, visual token pruning has emerged as a critical optimization strategy [10, 18], operating primarily across inter-frame and intra-frame dimensions. Inter-frame methods such as DTD [43] remove redundancy via pixel or feature differences, while intra-frame methods select or merge tokens using attention [9, 23, 41], diversity [3], token merging [7], or hybrid objectives [21]. However, these software-only cues are fragile for first-person dynamic spatial reasoning: appearance differences miss high-frequency motion continuity, attention scores suffer from peripheral spatial bias [40], and diversity or merging objectives can fragment local geometric structures. Consequently, existing pruning methods often discard motion- or structure-critical tokens under high compression.

Event-based Vision in VLMs. Event cameras (Dynamic Vision Sensors) asynchronously capture pixel-level brightness changes with microsecond resolution, offering intrinsic high dynamic range and motion sensitivity [15, 8, 36]. With recent commercialization by manufacturers such as Prophesee and Sony, these sensors are gaining traction in embodied AI applications including autonomous navigation and robotics. While demonstrating exceptional performance in vision tasks such as SLAM [35, 49], optical flow [48], and video reconstruction [16, 28], their integration into LVLMs remains limited. Recent event-LVLM methods such as EventCLIP [39], EventBind [47], and EventGPT [26] align event representations with vision-language embeddings or generate event-based captions, but typically require dedicated event encoders or additional training. In contrast, ECP uses events as a training-free score-level motion and structure prior for pruning visual tokens in existing RGB Video-LLMs, without parameter updates or event-embedding injection.

3 Methodology

Existing pruning methods [9, 41, 3, 21, 27] struggle to preserve both dynamics and geometry required for first-person dynamic spatial reasoning. Event cameras [15, 8] provide a lightweight external cue by recording asynchronous brightness changes that reveal motion activity and motion-induced structural cues. The key challenge lies in bridging the representational gap between asynchronous event streams and the synchronous grid features of Video-LLMs [5, 19]. We propose Event Cascade Pruning (ECP), a training-free framework shown in Figure 2, which cascades temporal-spatial-semantic pruning: ETCS selects keyframes, EMSF filters low-motion regions, and EARF fuses event saliency with attention-derived semantic scores for layer-wise token pruning.

3.1 Preliminaries

Attention-based Pruning. Token pruning reduces computational overhead by retaining the top- k tokens based on an importance score $\mathbf{s} \in \mathbb{R}^{T \times N}$. Existing methods [9, 41, 23] derive \mathbf{s} from

text-image attention weights:

$$\mathbf{S}_{\text{img}}^{(l)} = \frac{1}{m} \sum_{i=1}^m \text{Atten}^{(l)}(\mathbf{X}_I, \mathbf{X}_T^{(i)}) \quad (1)$$

where \mathbf{X}_I and \mathbf{X}_T denote image and text tokens, and m is the number of text tokens.

Event Camera as Motion Prior. Unlike frame-based sensors, event cameras [15] asynchronously trigger events $e_k = (\mathbf{u}_k, t_k, p_k)$ only when logarithmic intensity changes exceed a threshold:

$$|\ln I(\mathbf{u}, t) - \ln I(\mathbf{u}, t_{\text{prev}})| \geq \theta \quad (2)$$

The resulting stream \mathcal{E} offers microsecond-level temporal resolution, providing rich cues about motion causality and geometric boundaries that can be leveraged for spatial reasoning.

3.2 Event-Triggered Causal Sampling

Existing sampling strategies struggle to balance coverage and efficiency: uniform sampling misses transient dynamics, while appearance-based methods incur high computational cost and are sensitive to motion blur. We propose ETCS, a lightweight paradigm that leverages high-temporal-resolution event streams to anchor motion-rich moments and critical change points in scene dynamics.

Event Activity Flux. To align temporal sampling with non-uniform motion activity, we divide the event stream into fixed temporal windows $W_n = [n\Delta t, (n+1)\Delta t)$ indexed by n . Applying a spatiotemporal density filter $\Phi(\cdot)$ to mitigate sensor noise, we define the window-level activity flux as S_n . A larger S_n indicates stronger event activity within window n :

$$S_n = \sum_{k=1}^{|\mathcal{E}|} \Phi(e_k) \mathbb{I}[t_k \in W_n]. \quad (3)$$

Dual-Criteria Frame Anchoring. ETCS anchors frames using two complementary cues: high event activity S_n preserves motion-rich moments, while large activity changes indicate critical change points in scene dynamics:

$$\Delta S_n = |S_n - S_{n-1}|, \quad n \geq 1. \quad (4)$$

A large ΔS_n indicates that the event activity changes sharply between adjacent windows, and is therefore treated as a critical temporal anchor. Given the budget N_{target} , ETCS jointly selects high- S_n windows and top-ranked ΔS_n windows, then refines the set by pruning clustered low-activity candidates or filling large temporal gaps. The selected windows are mapped to the nearest RGB keyframes. Since both cues are computed on density-filtered window activity, ETCS suppresses event jitter while maintaining temporal coverage.

3.3 Event-guided Motion Saliency Filtering

Following temporal sampling, spatial redundancy remains a bottleneck. RGB-based motion differencing requires additional frame processing and can degrade under fast motion or blur, whereas event streams provide lightweight, high-temporal-resolution cues of local brightness changes. EMSF distills the event activity aligned with each selected keyframe into a token-aligned motion prior, enabling early suppression of event-inactive visual tokens.

Token-aligned Motion Saliency. For each selected keyframe f , let $\mathcal{W}_f = [a_f, a_f + \Delta t)$ denote its aligned event window. Each visual token $i \in \{1, \dots, N\}$ corresponds to a spatial support $\Omega_i^{(f)}$ in the image plane. Given the density-filtered event stream $\tilde{\mathcal{E}}$, we compute the event activity associated with token i as:

$$C_i^{(f)} = \sum_{e_k \in \tilde{\mathcal{E}}} \mathbb{I}[(x_k, y_k) \in \Omega_i^{(f)}, t_k \in \mathcal{W}_f], \quad M_i^{(f)} = \mathcal{N}_f(C_i^{(f)}), \quad (5)$$

where $\mathcal{N}_f(\cdot)$ denotes min-max normalization over all visual tokens in keyframe f . The resulting score $M_i^{(f)} \in [0, 1]$ measures the event-guided motion saliency of visual token i .

Budgeted Motion-token Retention. With retention ratio ρ , EMSF keeps $K = \lfloor \rho N \rfloor$ visual tokens per keyframe by maximizing the retained motion saliency:

$$\mathcal{I}_{\text{EMSF}}^{(f)} = \arg \max_{\mathcal{I} \subseteq \{1, \dots, N\}, |\mathcal{I}|=K} \sum_{i \in \mathcal{I}} M_i^{(f)}. \quad (6)$$

By reducing the number of visual tokens from N to K before subsequent attention, EMSF reduces the visual-token attention term from $O(N^2)$ to $O(K^2) = O(\rho^2 N^2)$ and provides motion-salient candidates for EARF.

3.4 Event-Attention Rank Alignment and Fusion

While EMSF suppresses event-inactive visual tokens, the remaining candidates still dominate subsequent attention and KV-cache storage [40, 22]. EARF further sparsifies these tokens at selected pruning layers \mathcal{L}_p by calibrating attention-based importance with event saliency. Importantly, events are used only to compute pruning scores and masks, rather than being encoded, concatenated with RGB embeddings, or injected into hidden representations.

Empirical Motivation: Peripheral Sink. Our analysis of 21,920 frames across 28 transformer layers (Figure 3) reveals a consistent *Peripheral Sink* in Video-LLMs [5]: visual attention concentrates more on image borders than on central regions, with the peripheral-to-center attention ratio exceeding 1 across all layers ($p < 10^{-10}$). This spatial bias resembles the attention sink observed in LLMs [40], but appears over peripheral visual tokens rather than initial text tokens. The bias is layer-dependent and is strongest in middle layers, where the ratio reaches $5.64 \times$. Moreover, the layer-wise bias profiles are highly correlated across datasets ($r = 0.897$), suggesting that the effect is largely model-intrinsic rather than dataset-specific. As a result, pruning solely by attention can preserve position-biased artifacts while discarding motion-relevant regions, motivating our event-guided rank calibration. Detailed per-layer statistics are provided in Appendix A.

Fusion via Rank Projection. Starting from the EMSF-retained candidates, EARF further sparsifies visual tokens at pruning layers \mathcal{L}_p . For pruning layer l and keyframe f , let $\mathcal{V}^{(l,f)}$ denote the active visual-token set before pruning. EARF first derives a text-conditioned visual importance score from the preceding post-softmax multimodal self-attention map:

$$A_i^{(l,f)} = \frac{1}{|\mathcal{Q}_s|} \sum_{q \in \mathcal{Q}_s} \mathbf{A}^{(l-1)}[q, i], \quad i \in \mathcal{V}^{(l,f)}. \quad (7)$$

Here \mathcal{Q}_s denotes the scoring query-token set used to read out visual importance, and $\mathbf{A}^{(l-1)}$ is the head-averaged post-softmax attention map used for scoring. The event-guided saliency $M_i^{(f)}$ is obtained from EMSF for the same visual token. Since attention scores and event saliency scores lie on different numerical scales and often exhibit long-tailed distributions (see Figure 8 in Appendix B), direct arithmetic fusion can be dominated by a few extreme tokens. EARF therefore projects both signals into a shared rank space within each keyframe:

$$R_{\mathcal{V}^{(l,f)}}(\phi, i) = \frac{\text{rank}_{\mathcal{V}^{(l,f)}}(\phi_i)}{\max(|\mathcal{V}^{(l,f)}| - 1, 1)}, \quad \phi \in \{A^{(l,f)}, M^{(f)}\}. \quad (8)$$

Here $\text{rank}_{\mathcal{V}^{(l,f)}}(\phi_i)$ denotes the zero-based ascending rank of token i among active visual tokens in $\mathcal{V}^{(l,f)}$, so larger scores receive larger normalized ranks. This non-parametric projection mitigates scale mismatch while preserving ordinal token importance.

Layer-wise Rank Calibration and Pruning. EARF computes the calibrated pruning score as:

$$S_{\text{calib}}^{(l,f,i)} = (1 - \gamma_l) R_{\mathcal{V}^{(l,f)}}(A^{(l,f)}, i) + \gamma_l R_{\mathcal{V}^{(l,f)}}(M^{(f)}, i). \quad (9)$$

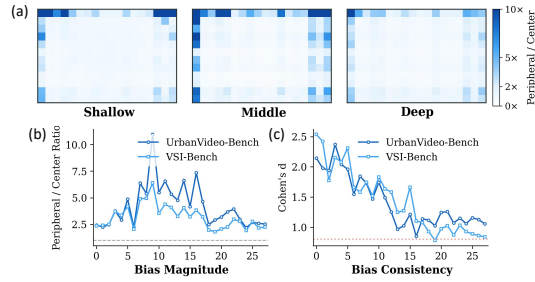


Figure 3: Peripheral Sink. (a) Attention maps reveal border-biased visual attention. (b) Peripheral-to-center ratio measures bias magnitude across layers. (c) Cohen’s d measures bias reliability, with similar trends across datasets.

The weight γ_l primarily follows the bias reliability measured by Cohen’s d (Figure 3(c)): high- d layers receive stronger event-guided correction, while deeper low- d layers use smaller γ_l to preserve content-dependent semantic attention.

Given the layer-wise retention ratio ρ_l , EARF keeps $K_l^{(f)} = \max(1, \lfloor \rho_l |\mathcal{V}^{(l,f)}| \rfloor)$ visual tokens with the highest calibrated scores in each keyframe:

$$\mathcal{I}_{\text{EARF}}^{(l,f)} = \arg \max_{\mathcal{I} \subseteq \mathcal{V}^{(l,f)}, |\mathcal{I}|=K_l^{(f)}} \sum_{i \in \mathcal{I}} S_{\text{calib}}^{(l,f,i)}. \quad (10)$$

By lowering the calibrated ranks of tokens whose attention scores are inflated by peripheral bias but lack event support, EARF makes such tokens less likely to be retained, reducing the presence of event-unsupported position-biased keys and values in the downstream KV cache. Appendix C provides a mechanistic interpretation of how EARF reduces event-unsupported position-biased keys and values in subsequent attention computation.

4 Experiments

We evaluate ECP on first-person dynamic spatial reasoning benchmarks using both simulated and real event streams. Our experiments address four questions: (1) Does ECP outperform existing pruning methods? (2) What are the computational gains? (3) Is ECP effective on both simulated and real events? (4) How does each component contribute?

4.1 Experimental Setup

Benchmarks. We focus on spatial reasoning during motion in 3D physical space and evaluate ECP in two event-stream settings. For public RGB-only benchmarks, we use VSI-Bench [42] (indoor navigation) and UrbanVideo-Bench [46] (outdoor drone scenarios). We focus on 13 ego-motion-centric tasks covering perception, cognition, and reasoning/planning, such as relative distance, proximity, route planning, and landmark positioning. Since these datasets lack native events, we generate simulated events offline with vid2e [16] from each original video at its native frame rate. ETCS uses the full simulated event stream for temporal scoring, while EMSF/EARF only use event windows aligned with the retained RGB keyframes. To further validate effectiveness on native event signals, we introduce ESR-Real, a synchronized RGB-event benchmark for first-person dynamic spatial reasoning with over 700 QA pairs across 6 categories (see Figure 4 for distribution). Dataset construction details are provided in Appendix E.

Baselines. We integrate ECP into Qwen2.5-VL-7B-Instruct [5] and compare with seven training-free baselines. Six of them are RGB-only pruning methods: DTD [43] uses inter-frame differencing; FastV [9], PyramidDrop [41], and VTW [23] use attention-based pruning; DivPrune [3] uses diversity-based pruning; and BTP [21] combines attention saliency with diversity. We also include Direct Event Pruning (DEP), an event-only baseline that directly uses token-aligned event density maps as pruning saliency under the same token budgets. DEP controls for whether improvements come from event access alone. All methods are evaluated at 70%, 50%, and 20% final visual-token retention relative to the unpruned model.

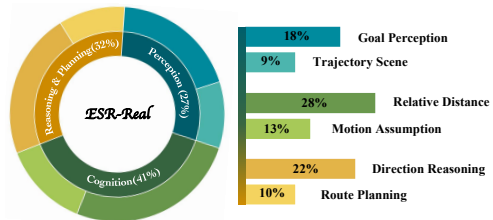


Figure 4: ESR-Real task distribution across Perception, Cognition, and Reasoning.

Implementation. Experiments run on NVIDIA A6000 GPUs with FlashAttention-2 [13] acceleration. All methods are implemented on the same codebase for fair comparison. Following standard practice in VLM evaluation [19, 42, 5], we use greedy decoding for deterministic inference. Event streams are aligned with visual tokens following the procedure described in Section 3.3. Pruning layers are determined by the layer-wise bias dynamics (Figure 3b): we intervene at stages preceding rapid bias escalation to preemptively correct attention drift before it propagates through the network. The fusion weight γ_l is modulated according to bias consistency (Figure 3c): layers with high and stable Cohen’s d receive stronger event-guided motion prior correction, while layers exhibiting content-dependent variation preserve greater semantic flexibility. We report inference latency, GFLOPs, and peak

Table 1: **Accuracy comparison on first-person dynamic spatial reasoning benchmarks.** Avg.Acc is computed over all 13 selected tasks; six representative task columns are shown here and the remaining seven are reported in Appendix F. Best in bold. *Task definitions: SE.Pos=Start/End Position; Goal.Det=Goal Detection; Rel.Dis=Relative Distance; Proximity=Proximity Estimation; Ass.Reason=Association Reasoning; Landmark.Pos=Landmark Positioning.*

Method	Avg.Acc	Perception		Cognition		Reasoning & Planning	
		SE.Pos	Goal.Det	Rel.Dis	Proximity	Ass.Reason	Landmark.Pos
Original	36.31	55.10	39.79	44.51	50.00	16.90	37.41
<i>70% Retaining</i>							
DTD	36.36	55.10	39.44	42.63	46.88	15.96	37.76
FastV	36.28	57.14	39.08	44.51	50.00	16.90	37.41
PDrop	36.73	53.06	40.49	44.83	46.88	15.96	36.71
DivPrune	36.16	55.10	39.79	43.26	46.88	15.96	37.06
BTP	35.95	57.14	39.44	43.26	46.88	17.37	36.71
VTW	36.45	57.14	39.44	44.83	50.00	17.84	36.71
DEP	36.88	53.10	38.30	45.80	50.00	18.80	37.80
OURS	37.78	59.18	40.49	49.22	56.25	17.37	37.76
<i>50% Retaining</i>							
DTD	36.55	59.18	39.44	42.01	53.12	17.37	35.31
FastV	35.67	51.02	37.32	42.32	46.88	17.37	37.06
PDrop	35.67	51.02	39.79	41.69	46.88	16.43	37.41
DivPrune	36.77	48.98	39.79	44.51	46.88	18.31	35.31
BTP	35.09	51.02	40.49	40.13	50.00	15.96	35.66
VTW	33.84	42.86	33.45	38.87	53.12	14.08	34.97
DEP	33.28	38.80	32.80	38.20	53.10	15.00	34.60
OURS	38.16	59.18	42.25	50.47	53.12	18.78	37.06
<i>20% Retaining</i>							
DTD	35.37	51.02	37.68	39.50	50.00	16.43	35.31
FastV	32.64	28.57	29.58	33.23	46.88	14.55	31.82
PDrop	33.12	26.53	31.69	33.86	46.88	15.96	32.52
DivPrune	34.40	32.65	36.97	36.36	56.25	16.90	34.62
BTP	33.34	30.61	33.10	35.11	56.25	12.68	33.92
VTW	30.50	20.41	32.75	36.36	53.12	13.15	32.17
DEP	29.95	22.40	30.70	36.10	59.40	12.20	30.10
OURS	37.62	55.10	38.03	44.20	56.25	20.19	36.36

memory. For RGB-only public benchmarks, offline vid2e synthesis is excluded from the reported inference cost.

4.2 Main Results

Accuracy Comparison. Table 1 reveals distinct patterns across compression levels. At 70% retention, all methods remain competitive—the large token pool provides redundancy for baselines to capture useful tokens. As compression intensifies, this tolerance vanishes: at 20%, attention-based methods drop sharply (FastV: 32.64%, VTW: 30.50%), while ECP maintains 37.62%, surpassing even the full-token baseline (36.31%). Although DEP utilizes the same event modality, it suffers severe accuracy degradation at 50% (33.28%) and 20% (29.95%) retention. At 20% retention, DEP trails ECP by 7.67 percentage points. This suggests that our performance gains stem from the proposed semantic alignment and cascade architecture, rather than an advantage from simply introducing the event modality.

Task-wise analysis reveals where event-assisted pruning excels. For motion-dependent tasks like Rel.Dis, ECP achieves 44.20% at 20% retention—nearly matching the unpruned baseline (44.51%)—while baselines drop to 33–39%. In geometry-reliant tasks like SE.Pos, DEP plummets to a mere 22.40%. In contrast, ECP matches the full-token performance at 55.10%. These tasks require continuous motion tracking and boundary perception, precisely what event cameras capture. In contrast, Landmark.Pos shows smaller margins, as landmark localization relies on static scene memory rather than dynamic cues.

To validate effectiveness on real sensors, we evaluate on ESR-Real (Table 2). At 50% retention, ECP achieves 54.58%, surpassing the full-token baseline (51.90%) by 2.68%. Under more aggressive 20% retention, ECP remains the most robust pruning method, outperforming the second-best baseline (DTD: 46.40%) by 3.67%.

Table 2: **Accuracy comparison on ESR-Real benchmark.** ECP demonstrates consistent effectiveness on real event streams captured by physical sensors. Best in bold. *Task definitions: Goal.Percept=Goal Perception; Traj.Scene=Trajectory Scene; Rel.Dis=Relative Distance; Motion.Ass=Motion Assumption; Dir.Rea=Direction Reasoning; Route.Plan=Route Planning.*

Method	Avg.Acc	Perception		Cognition		Reasoning & Planning	
		Goal.Percept	Traj.Scene	Rel.Dis	Motion.Ass	Dir.Rea	Route.Plan
Original	51.90	63.28	31.75	69.35	39.56	30.82	63.77
<i>70% Retaining</i>							
DTD	51.20	65.62	28.57	67.34	35.16	30.82	66.67
FastV	51.48	62.50	34.92	68.34	37.36	30.82	63.77
PDrop	51.20	60.94	30.16	69.85	37.36	29.56	66.67
DivPrune	50.92	62.50	33.33	68.84	38.46	27.67	63.77
BTP	50.21	60.94	31.75	68.34	36.26	28.30	63.77
VTW	50.78	57.81	31.75	69.85	37.36	29.56	66.67
DEP	50.60	60.20	28.60	68.30	37.40	29.60	68.10
OURS	52.89	64.06	38.10	68.84	39.56	30.82	68.12
<i>50% Retaining</i>							
DTD	49.51	64.06	28.57	65.83	34.07	26.42	68.12
FastV	48.94	63.28	31.75	64.32	36.26	26.42	62.32
PDrop	50.49	63.28	33.33	65.83	37.36	29.56	63.77
DivPrune	50.21	65.62	30.16	64.82	40.66	27.67	62.32
BTP	50.21	63.28	34.92	64.32	38.46	28.30	65.22
VTW	43.58	64.84	26.98	47.24	31.87	28.30	59.42
DEP	41.50	64.80	27.00	42.70	27.50	27.00	59.40
OURS	54.58	67.97	38.10	69.85	40.66	32.70	69.57
<i>20% Retaining</i>							
DTD	46.40	66.41	25.40	55.78	34.07	27.04	62.32
FastV	39.77	66.41	20.63	37.19	34.07	25.79	55.07
PDrop	39.49	66.41	23.81	29.65	38.46	28.30	59.42
DivPrune	45.56	67.19	28.57	48.24	35.16	31.45	59.42
BTP	43.30	66.41	20.63	49.25	34.07	25.16	57.97
VTW	39.07	62.50	23.81	28.64	35.16	33.96	56.52
DEP	40.20	65.60	28.60	29.10	37.40	34.60	52.20
OURS	50.07	67.19	31.75	60.30	38.46	28.93	69.57

Efficiency Analysis. Table 3 reports online inference cost with event streams available either natively or precomputed. At 20% retention, ECP achieves 1.11s latency (1.89× speedup), 141.9 GFLOPs (52% reduction), and 16637 MB memory. Unlike DTD’s pixel-wise differencing or DivPrune’s $O(N^2)$ pairwise distances, ECP’s sparse event accumulation provides motion-aware guidance with low overhead. For RGB-only public benchmarks, offline vid2e generation is used only to construct the simulated-event evaluation setting and is excluded from the reported inference cost.

Table 3: Efficiency comparison on the UrbanVideo-Bench (20% retention ratio).

Method	Ratio	Time (s)	GFLOPs ↓	Mem (MB)
Full Tokens	-	2.10	294.6	18848
DTD	20%	1.80	185.9	16880
FastV	20%	1.16	173.9	17068
VTW	20%	1.18	189.8	17200
PDrop	20%	1.24	187.5	17169
DivPrune	20%	1.25	187.1	17169
BTP	20%	1.55	187.5	17169
Ours	20%	1.11	141.9	16637



Figure 5: **Qualitative comparison.** ECP retains physical structures even at high token compression.

Qualitative Analysis. Figure 5 visualizes token retention under high compression. Attention-based pruning (row 2) concentrates tokens at image borders, discarding the central sofa and chair critical for spatial judgment. Diversity-based pruning (row 3) fragments object boundaries into isolated

patches, breaking geometric continuity. ECP (row 4) anchors tokens at regions exhibiting high motion saliency, preserving continuous object contours and enabling correct spatial reasoning.

4.3 Ablation Studies

We conduct ablation studies to validate each component and design choice, examining three aspects: module contribution, fusion weight strategy, and layer selection.

Component Contribution. Table 4 reports component ablations averaged over the three retention ratios. ETCS mainly improves efficiency, reducing latency from 2.08s to 1.58s while slightly improving accuracy by 0.21 points. EMSF and EARF improve accuracy by 0.91 and 0.84 points individually. Adding ETCS to EMSF or EARF further improves accuracy, while EMSF+EARF without ETCS is less effective, suggesting that temporal anchoring is important for coherent event-attention fusion. The full cascade achieves the best measured trade-off, with 37.85% accuracy and 1.16s latency. Appendix G provides task-category breakdowns.

Table 4: Component ablation.

ETCS	EMSF	EARF	Lat.(s)	Acc.(%)
-	-	-	2.08	36.31
✓	-	-	1.58	36.52
-	✓	-	1.83	37.22
-	-	✓	1.53	37.15
✓	✓	-	1.47	37.51
✓	-	✓	1.17	37.75
-	✓	✓	1.59	37.00
✓	✓	✓	1.16	37.85

Fusion Weight Analysis. Table 5 examines the layer-wise fusion weight γ_l with pruning layers fixed. Three trends emerge: (1) Increasing the uniform event weight improves accuracy from 34.18% to 37.47% up to $\gamma = 0.7$, while event-only rank fusion ($\gamma = 1.0$) slightly drops to 37.36%, indicating that semantic attention remains complementary. (2) The shallow-heavy Decay pattern (0.8 \rightarrow 0.5 \rightarrow 0.3) outperforms Growth (0.3 \rightarrow 0.5 \rightarrow 0.8) by 1.05 points. (3) The bias-guided schedule (0.8, 0.6, 0.5) achieves the best accuracy of 37.62%. This aligns with Figure 3(c): high- d shallow layers receive stronger event-guided calibration, whereas lower- d deeper layers use smaller γ_l to preserve content-dependent semantic attention.

Table 5: Layer-wise fusion-weight ablation at 20% retention (S/M/D: shallow/mid/deep).

Strategy	γ_S	γ_M	γ_D	Acc.(%)	Analysis
Uniform	0.0	0.0	0.0	34.18	Baseline (Attn)
	0.3	0.3	0.3	35.66	Weak Fusion
	0.5	0.5	0.5	36.21	Medium Fusion
	0.7	0.7	0.7	37.47	Strong Fusion
	1.0	1.0	1.0	37.36	Pure Event
Peak (\wedge)	0.2	0.6	0.2	34.60	Mid-focus
Valley (\vee)	0.6	0.2	0.6	36.32	Ends-focus
Growth (\nearrow)	0.3	0.5	0.8	35.99	Suboptimal
Decay (\searrow)	0.8	0.5	0.3	37.04	Supports Hyp.
Best	0.8	0.6	0.5	37.62	Best Balance

Layer Selection Strategy. Table 6 compares our bias-guided layer selection against uniform layer spacing, both using the same ECP modules and final token budgets. Uniform is marginally higher at 70% retention (38.10 vs. 37.78), suggesting a token-buffer regime where near-full spatial coverage can preserve task-critical cues and mask suboptimal layer placement. Once this buffer vanishes, stability becomes decisive: uniform spacing drops 3.24 points from 70% to 20% retention (38.10 \rightarrow 34.86), whereas our bias-guided placement drops only 0.16 points (37.78 \rightarrow 37.62). These suggest that bias-guided layer selection mainly targets extreme-sparsity stability by intervening before peripheral-bias escalation propagates through the residual stream and KV cache.

Table 6: Layer selection ablation.

Ratio	Variant	Avg.	Urban	VSI
Full	Baseline	36.31	40.86	32.03
70%	Uniform	38.10	42.91	33.13
70%	Ours	37.78	42.49	33.35
50%	Uniform	37.09	42.56	29.88
50%	Ours	38.16	42.85	33.76
20%	Uniform	34.86	39.99	29.77
20%	Ours	37.62	42.78	32.76

5 Conclusion and Limitations

We presented Event Cascade Pruning (ECP), a training-free event-assisted pruning framework for efficient first-person dynamic spatial reasoning. By cascading event-triggered sampling, motion-saliency filtering, and event-attention rank fusion, ECP converts high-frequency event cues into pruning decisions that preserve dynamic and geometric structures under high compression. At 20% token retention, ECP surpasses the full-token baseline (37.62% vs. 36.31%) with 1.89 \times speedup and 52% GFLOPs reduction; on ESR-Real, it gains 2.68 points at 50% retention. We will release the code and ESR-Real dataset upon publication.

Limitations. ECP assumes synchronized RGB-event inputs; it targets platforms where an event camera is paired with RGB sensing, rather than serving as an RGB-only online acceleration method. Although event sensors remain less ubiquitous than RGB cameras, commercialization by Sony and Prophesee makes this setting increasingly feasible. More broadly, ECP illustrates sensor-assisted pruning and motivates future external-prior-guided or RGB-only distilled pruning schemes.

References

- [1] Josh Achiam, Steven Adler, Sandhini Agarwal, Lama Ahmad, Ilge Akkaya, Florencia Leoni Aleman, Diogo Almeida, Janko Altschmidt, Sam Altman, Shyamal Anadkat, et al. Gpt-4 technical report. *arXiv preprint arXiv:2303.08774*, 2023.
- [2] Jean-Baptiste Alayrac, Jeff Donahue, Pauline Luc, Antoine Miech, Iain Barr, Yana Hasson, Karel Lenc, Arthur Mensch, Katherine Millican, Malcolm Reynolds, et al. Flamingo: a visual language model for few-shot learning. *Advances in neural information processing systems*, 35:23716–23736, 2022.
- [3] Saeed Ranjbar Alvar, Gursimran Singh, Mohammad Akbari, and Yong Zhang. Divprune: Diversity-based visual token pruning for large multimodal models. In *Proceedings of the Computer Vision and Pattern Recognition Conference*, pages 9392–9401, 2025.
- [4] Shuai Bai, Yuxuan Cai, Ruizhe Chen, Keqin Chen, Xionghui Chen, Zesen Cheng, Lianghao Deng, Wei Ding, Chang Gao, Chunjiang Ge, et al. Qwen3-vl technical report. *arXiv preprint arXiv:2511.21631*, 2025.
- [5] Shuai Bai, Keqin Chen, Xuejing Liu, Jialin Wang, Wenbin Ge, Sibao Song, Kai Dang, Peng Wang, Shijie Wang, and Jun Tang. Qwen2.5-vl technical report. 2025.
- [6] Jing Bi, Yunlong Tang, Luchuan Song, Ali Vosoughi, Nguyen Nguyen, and Chenliang Xu. Eagle: Egocentric aggregated language-video engine. *arXiv preprint arXiv:2409.17523*, 2024.
- [7] Daniel Bolya, Cheng-Yang Fu, Xiaoliang Dai, Peizhao Zhang, Christoph Feichtenhofer, and Judy Hoffman. Token merging: Your vit but faster. *arXiv preprint arXiv:2210.09461*, 2022.
- [8] Bharatesh Chakravarthi, Aayush Atul Verma, Kostas Daniilidis, Cornelia Fermuller, and Yezhou Yang. Recent event camera innovations: A survey. In *European conference on computer vision*, pages 342–376. Springer, 2024.
- [9] Liang Chen, Haozhe Zhao, Tianyu Liu, Shuai Bai, Junyang Lin, Chang Zhou, and Baobao Chang. An image is worth 1/2 tokens after layer 2: Plug-and-play inference acceleration for large vision-language models. In *European Conference on Computer Vision*, pages 19–35. Springer, 2024.
- [10] Xuanyao Chen, Zhijian Liu, Haotian Tang, Li Yi, Hang Zhao, and Song Han. Sparsevit: Revisiting activation sparsity for efficient high-resolution vision transformer. In *Proceedings of the IEEE/CVF conference on computer vision and pattern recognition*, pages 2061–2070, 2023.
- [11] Zhe Chen, Jiannan Wu, Wenhai Wang, Weijie Su, Guo Chen, Sen Xing, Muyan Zhong, Qinglong Zhang, Xizhou Zhu, Lewei Lu, et al. Internvl: Scaling up vision foundation models and aligning for generic visual-linguistic tasks. In *Proceedings of the IEEE/CVF conference on computer vision and pattern recognition*, pages 24185–24198, 2024.
- [12] Ronghao Dang, Yuqian Yuan, Yunxuan Mao, Kehan Li, Jiangpin Liu, Zhikai Wang, Xin Li, Fan Wang, and Deli Zhao. Rynnc: Bringing mllms into embodied world. *arXiv preprint arXiv:2508.14160*, 2025.
- [13] Tri Dao. Flashattention-2: Faster attention with better parallelism and work partitioning. *arXiv preprint arXiv:2307.08691*, 2023.
- [14] Yue Fan, Xiaojuan Ma, Rongpeng Su, Jun Guo, Rujie Wu, Xi Chen, and Qing Li. Embodied videoagent: Persistent memory from egocentric videos and embodied sensors enables dynamic scene understanding. In *2025 IEEE/CVF International Conference on Computer Vision (ICCV)*, pages 6342–6352. IEEE, 2025.
- [15] Guillermo Gallego, Tobi Delbrück, Garrick Orchard, Chiara Bartolozzi, Brian Taba, Andrea Censi, Stefan Leutenegger, Andrew J Davison, Jörg Conradt, Kostas Daniilidis, et al. Event-based vision: A survey. *IEEE transactions on pattern analysis and machine intelligence*, 44(1):154–180, 2020.
- [16] Daniel Gehrig, Mathias Gehrig, Javier Hidalgo-Carrió, and Davide Scaramuzza. Video to events: Recycling video datasets for event cameras. In *Proceedings of the IEEE/CVF conference on computer vision and pattern recognition*, pages 3586–3595, 2020.

- [17] Xiaohu Huang, Hao Zhou, and Kai Han. Prunevid: Visual token pruning for efficient video large language models. In *Findings of the Association for Computational Linguistics: ACL 2025*, pages 19959–19973, 2025.
- [18] Huiqiang Jiang, Qianhui Wu, Chin-Yew Lin, Yuqing Yang, and Lili Qiu. Llmlingua: Compressing prompts for accelerated inference of large language models. In *Proceedings of the 2023 conference on empirical methods in natural language processing*, pages 13358–13376, 2023.
- [19] Bo Li, Yuanhan Zhang, Dong Guo, Renrui Zhang, Feng Li, Hao Zhang, Kaichen Zhang, Peiyuan Zhang, Yanwei Li, Ziwei Liu, et al. Llava-onevision: Easy visual task transfer. *arXiv preprint arXiv:2408.03326*, 2024.
- [20] Junnan Li, Dongxu Li, Silvio Savarese, and Steven Hoi. Blip-2: Bootstrapping language-image pre-training with frozen image encoders and large language models. In *International conference on machine learning*, pages 19730–19742. PMLR, 2023.
- [21] Kaiyuan Li, Xiaoyue Chen, Chen Gao, Yong Li, and Xinlei Chen. Balanced token pruning: Accelerating vision language models beyond local optimization. *arXiv preprint arXiv:2505.22038*, 2025.
- [22] Yuhong Li, Yingbing Huang, Bowen Yang, Bharat Venkitesh, Acyr Locatelli, Hanchen Ye, Tianle Cai, Patrick Lewis, and Deming Chen. Snapkv: Llm knows what you are looking for before generation. *Advances in Neural Information Processing Systems*, 37:22947–22970, 2024.
- [23] Zhihang Lin, Mingbao Lin, Luxi Lin, and Rongrong Ji. Boosting multimodal large language models with visual tokens withdrawal for rapid inference. In *Proceedings of the AAAI Conference on Artificial Intelligence*, volume 39, pages 5334–5342, 2025.
- [24] Haotian Liu, Chunyuan Li, Qingyang Wu, and Yong Jae Lee. Visual instruction tuning. *Advances in neural information processing systems*, 36:34892–34916, 2023.
- [25] Haotian Liu, Chunyuan Li, Yuheng Li, Bo Li, Yuanhan Zhang, Sheng Shen, and Yong Jae Lee. Lllavanext: Improved reasoning, ocr, and world knowledge, 2024.
- [26] Shaoyu Liu, Jianing Li, Guanghui Zhao, Yunjian Zhang, Xin Meng, Fei Richard Yu, Xiangyang Ji, and Ming Li. Eventgpt: Event stream understanding with multimodal large language models. In *Proceedings of the Computer Vision and Pattern Recognition Conference*, pages 29139–29149, 2025.
- [27] Yongming Rao, Wenliang Zhao, Benlin Liu, Jiwen Lu, Jie Zhou, and Cho-Jui Hsieh. Dynamicvit: Efficient vision transformers with dynamic token sparsification. *Advances in neural information processing systems*, 34:13937–13949, 2021.
- [28] Henri Rebecq, René Ranftl, Vladlen Koltun, and Davide Scaramuzza. High speed and high dynamic range video with an event camera. *IEEE transactions on pattern analysis and machine intelligence*, 43(6): 1964–1980, 2019.
- [29] Henri Rebecq, René Ranftl, Vladlen Koltun, and Davide Scaramuzza. Events-to-video: Bringing modern computer vision to event cameras. In *Proceedings of the IEEE/CVF conference on computer vision and pattern recognition*, pages 3857–3866, 2019.
- [30] Adarsh Jagan Sathyamoorthy, Kasun Weerakoon, Mohamed Elnoor, Anuj Zore, Brian Ichter, Fei Xia, Jie Tan, Wenhao Yu, and Dinesh Manocha. Convoi: Context-aware navigation using vision language models in outdoor and indoor environments. In *2024 IEEE/RSJ International Conference on Intelligent Robots and Systems (IROS)*, pages 13837–13844. IEEE, 2024.
- [31] Xiaoqian Shen, Yunyang Xiong, Changsheng Zhao, Lemeng Wu, Jun Chen, Chenchen Zhu, Zechun Liu, Fanyi Xiao, Balakrishnan Varadarajan, Florian Bordes, et al. Longvu: Spatiotemporal adaptive compression for long video-language understanding. *arXiv preprint arXiv:2410.17434*, 2024.
- [32] Alessandro Suglia, Claudio Greco, Katie Baker, Jose L Part, Ioannis Papaioannou, Arash Eshghi, Ioannis Konstantas, and Oliver Lemon. Alanavlm: A multimodal embodied ai foundation model for egocentric video understanding. In *Findings of the Association for Computational Linguistics: EMNLP 2024*, pages 11101–11122, 2024.
- [33] Jacob Thompson, Emiliano Garcia-Lopez, and Yonatan Bisk. Rem: Evaluating llm embodied spatial reasoning through multi-frame trajectories. *arXiv preprint arXiv:2512.00736*, 2025.
- [34] Hugo Touvron, Louis Martin, Kevin Stone, Peter Albert, Amjad Almahairi, Yasmine Babaei, Nikolay Bashlykov, Soumya Batra, Prajjwal Bhargava, Shrutu Bhosale, et al. Llama 2: Open foundation and fine-tuned chat models. *arXiv preprint arXiv:2307.09288*, 2023.

- [35] Antoni Rosinol Vidal, Henri Rebecq, Timo Horstschaefer, and Davide Scaramuzza. Ultimate slam? combining events, images, and imu for robust visual slam in hdr and high-speed scenarios. *IEEE Robotics and Automation Letters*, 3(2):994–1001, 2018.
- [36] Haoyang Wang, Ruishan Guo, Pengtao Ma, Ciyu Ruan, Xinyu Luo, Wenhua Ding, Tianyang Zhong, Jingao Xu, Yunhao Liu, and Xinlei Chen. Event camera meets mobile embodied perception: abstraction, algorithm, acceleration, application. *ACM Computing Surveys*, 58(8):1–41, 2026.
- [37] Weihang Wang, Qingsong Lv, Wenmeng Yu, Wenyi Hong, Ji Qi, Yan Wang, Junhui Ji, Zhuoyi Yang, Lei Zhao, Xixuan Song, et al. Cogvlm: Visual expert for pretrained language models. *Advances in Neural Information Processing Systems*, 37:121475–121499, 2024.
- [38] Shiwei Wu, Joya Chen, Kevin Qinghong Lin, Qimeng Wang, Yan Gao, Qianli Xu, Tong Xu, Yao Hu, Enhong Chen, and Mike Zheng Shou. Videollm-mod: Efficient video-language streaming with mixture-of-depths vision computation. *Advances in Neural Information Processing Systems*, 37:109922–109947, 2024.
- [39] Ziyi Wu, Xudong Liu, and Igor Gilitschenski. Eventclip: Adapting clip for event-based object recognition. *arXiv preprint arXiv:2306.06354*, 2023.
- [40] Guangxuan Xiao, Yuandong Tian, Beidi Chen, Song Han, and Mike Lewis. Efficient streaming language models with attention sinks. *arXiv preprint arXiv:2309.17453*, 2023.
- [41] Long Xing, Qidong Huang, Xiaoyi Dong, Jiajie Lu, Pan Zhang, Yuhang Zang, Yuhang Cao, Conghui He, Jiaqi Wang, Feng Wu, et al. Pyramidrop: Accelerating your large vision-language models via pyramid visual redundancy reduction. *arXiv preprint arXiv:2410.17247*, 2024.
- [42] Jihan Yang, Shusheng Yang, Anjali W Gupta, Rilyn Han, Li Fei-Fei, and Saining Xie. Thinking in space: How multimodal large language models see, remember, and recall spaces. In *Proceedings of the Computer Vision and Pattern Recognition Conference*, pages 10632–10643, 2025.
- [43] Linli Yao, Yicheng Li, Yuancheng Wei, Lei Li, Shuhuai Ren, Yuanxin Liu, Kun Ouyang, Lean Wang, Shicheng Li, Sida Li, et al. Timechat-online: 80% visual tokens are naturally redundant in streaming videos. In *Proceedings of the 33rd ACM International Conference on Multimedia*, pages 10807–10816, 2025.
- [44] Jiazhaoh Zhang, Kunyu Wang, Shaoan Wang, Minghan Li, Haoran Liu, Songlin Wei, Zhongyuan Wang, Zhizheng Zhang, and He Wang. Uni-navid: A video-based vision-language-action model for unifying embodied navigation tasks. *arXiv preprint arXiv:2412.06224*, 2024.
- [45] Zhengyou Zhang. A flexible new technique for camera calibration. *IEEE Transactions on pattern analysis and machine intelligence*, 22(11):1330–1334, 2000.
- [46] Baining Zhao, Jianjie Fang, Zichao Dai, Ziyong Wang, Jirong Zha, Weichen Zhang, Chen Gao, Yue Wang, Jinqiang Cui, Xinlei Chen, et al. Urbanvideo-bench: Benchmarking vision-language models on embodied intelligence with video data in urban spaces. In *Proceedings of the 63rd Annual Meeting of the Association for Computational Linguistics (Volume 1: Long Papers)*, pages 32400–32423, 2025.
- [47] Jiazhou Zhou, Xu Zheng, Yuanhuiyi Lyu, and Lin Wang. Eventbind: Learning a unified representation to bind them all for event-based open-world understanding. In *European Conference on Computer Vision*, pages 477–494. Springer, 2024.
- [48] Alex Zihao Zhu, Liangzhe Yuan, Kenneth Chaney, and Kostas Daniilidis. Ev-flownet: Self-supervised optical flow estimation for event-based cameras. *arXiv preprint arXiv:1802.06898*, 2018.
- [49] Alex Zihao Zhu, Liangzhe Yuan, Kenneth Chaney, and Kostas Daniilidis. Unsupervised event-based learning of optical flow, depth, and egomotion. In *Proceedings of the IEEE/CVF conference on computer vision and pattern recognition*, pages 989–997, 2019.

A Spatial Attention Bias Analysis

This appendix provides statistical analysis of the spatial attention bias in vision-language models. We analyze 21,920 frames across all 28 transformer layers from UrbanVideo-Bench (472 videos, 15,104 frames) and VSI-Bench (213 videos, 6,816 frames).

A.1 Spatial Region Definition

All attention patterns are standardized onto a 12×18 spatial grid (216 tokens). As illustrated in Figure 6, we partition this grid into three regions using a 15% margin threshold: Corner (8 tokens, 3.7%), Edge (68 tokens, 31.5%), and Center (140 tokens, 64.8%). The Peripheral region (Corner \cup Edge, 76 tokens, 35.2%) serves as the primary metric for quantifying spatial attention bias.

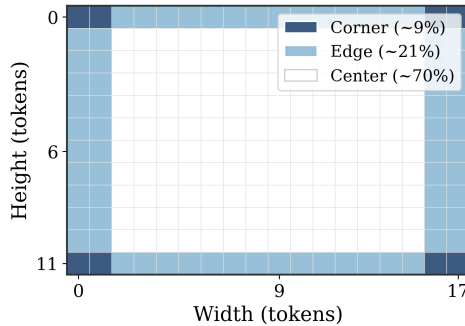


Figure 6: Spatial region partitioning. Peripheral = Corner (3.7%) + Edge (31.5%); Center (64.8%) serves as baseline.

A.2 Statistical Analysis

Table 7 provides complete per-layer statistics; Table 8 summarizes bias characteristics by layer group.

Table 7: Complete layer-wise statistics ($n = 21,920$). t : one-sample t -statistic against $\mu_0 = 1.0$; all layers satisfy $p < 10^{-10}$.

L	Corner	Edge	Periph.	d	t	L	Corner	Edge	Periph.	d	t
0	7.70	1.80	2.41	2.24	331	14	13.70	4.90	5.82	0.99	146
1	7.00	1.80	2.31	2.09	310	15	9.00	3.30	3.87	1.23	182
2	7.60	1.90	2.48	1.88	279	16	12.60	5.50	6.25	0.80	118
3	12.30	2.70	3.75	2.30	341	17	9.70	3.50	4.20	1.08	160
4	9.20	2.30	3.05	2.01	297	18	4.00	2.10	2.33	1.04	154
5	16.80	3.20	4.66	1.99	295	19	3.80	2.40	2.57	0.91	134
6	6.40	1.70	2.18	1.56	231	20	5.00	2.60	2.84	1.10	163
7	20.30	4.20	5.92	1.72	254	21	8.10	2.70	3.23	1.11	165
8	19.40	3.60	5.26	1.73	256	22	10.20	2.90	3.64	1.00	148
9	47.70	5.00	9.53	1.35	200	23	7.30	2.40	2.92	1.11	164
10	18.90	3.20	4.89	1.59	235	24	4.40	1.80	2.11	1.01	150
11	18.00	4.50	5.89	1.41	209	25	6.30	2.30	2.72	1.04	154
12	12.40	4.10	4.95	1.26	187	26	5.70	2.10	2.47	1.04	153
13	8.00	3.90	4.31	0.95	141	27	5.90	2.00	2.44	0.98	145

Table 8: Summary statistics by layer group.

Group	Layers	Periph.	Corner	Edge	d
Shallow	0–7	$3.35 \times$	$10.20 \times$	$2.40 \times$	1.97
Middle	8–16	$5.64 \times$	$22.80 \times$	$4.20 \times$	1.26
Deep	17–27	$2.86 \times$	$6.10 \times$	$2.30 \times$	1.04

Key findings from Table 7: (1) All 28 layers show significant peripheral bias ($p < 10^{-10}$). (2) Layer 9 exhibits peak ratio ($9.53\times$); Layer 3 achieves highest d (2.30). (3) Mean ratio across layers is $3.89\times$. (4) Cross-dataset correlation $r = 0.897$ ($p < 10^{-10}$) confirms this is a model-intrinsic property.

A.3 Effect Size Interpretation

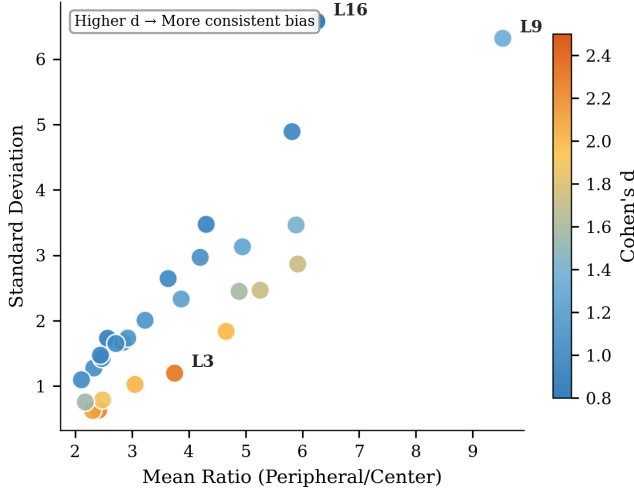


Figure 7: Bias magnitude vs. consistency. Cohen’s $d = (\mu - 1)/\sigma$ penalizes variance: Layer 9 has peak ratio ($9.53\times$) but moderate d (1.35); Layer 3 achieves highest d (2.30) with lower ratio ($3.75\times$).

Figure 7 shows why high bias magnitude does not imply high effect size. Layers with high Cohen’s d provide more reliable pruning decisions due to consistent bias patterns.

A.4 Design Implications

Pruning Layer Selection. Effective pruning layers should satisfy two criteria: (1) intervene before bias escalation to prevent error propagation, and (2) exhibit high Cohen’s d for reliable decisions. The ablation study empirically validates this strategy.

Fusion Weight γ_l . Shallow layers exhibit the highest consistency ($d = 1.97$), making event-based calibration most reliable there. We adopt a decay schedule where γ_l decreases from shallow to deep layers. The ablation study empirically validates this strategy.

B Long-tailed Distribution Analysis

This appendix analyzes the distributional properties of attention scores and event density, which motivates our rank-based fusion strategy in EARF (Section 3.4).

As shown in Figure 8, both attention scores and event density exhibit severe long-tailed distributions: a small fraction of tokens dominate the score mass while the majority cluster near zero. This distributional skewness poses a fundamental challenge for multimodal fusion—direct arithmetic combination (e.g., weighted sum) would be dominated by outliers from either modality, failing to capture the relative importance across the full token population. Our rank-based projection normalizes these skewed distributions into uniform ranks, enabling fair comparison and robust fusion.

C Mechanistic Analysis of KV-Cache Purification

This appendix provides an analytical interpretation of how event-unsupported peripheral sink tokens can degrade downstream key–value states in Video-LLMs, and how EARF mitigates this issue through event-assisted rank calibration. We use “KV cache” broadly to refer to the active keys and values retained for subsequent attention computation.

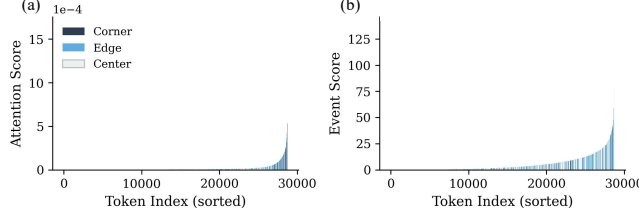


Figure 8: Long-tailed distribution of attention scores and event density. Both modalities exhibit severe skewness, motivating rank-based fusion.

C.1 Problem: Peripheral Sink Tokens in the KV Cache

For clarity, we focus on one pruning layer l . EARF performs score calibration and top- K pruning within each keyframe, but the retained tokens are then merged into the active sequence for subsequent multimodal self-attention. Let $\mathcal{T}^{(l)}$ denote the always-retained text and special tokens, and let $\mathcal{V}^{(l)} = \bigcup_f \mathcal{V}^{(l,f)}$ denote all active visual tokens before pruning, where $\mathcal{V}^{(l,f)}$ is the active visual-token set of keyframe f . The active key-value set is:

$$\mathcal{K}^{(l)} = \mathcal{T}^{(l)} \cup \mathcal{V}^{(l)}. \quad (11)$$

For a query vector q , attention over the global active set $\mathcal{K}^{(l)}$ produces:

$$z_q^{(l)} = \sum_{i \in \mathcal{K}^{(l)}} \alpha_{q,i}^{(l)} v_i^{(l)}, \quad \alpha_{q,i}^{(l)} = \frac{\exp\left(q^\top k_i^{(l)} / \sqrt{d_k}\right)}{\sum_{j \in \mathcal{K}^{(l)}} \exp\left(q^\top k_j^{(l)} / \sqrt{d_k}\right)}, \quad (12)$$

where d_k denotes the key dimension. Pruning changes only the visual-token subset of $\mathcal{K}^{(l)}$, while text and special tokens are always kept.

As demonstrated in Appendix A, visual attention in the evaluated Video-LLM exhibits a consistent peripheral sink: border and corner tokens receive inflated attention scores relative to central tokens. Let $\mathcal{P}^{(l,f)} \subseteq \mathcal{V}^{(l,f)}$ denote event-unsupported peripheral visual tokens in keyframe f , and let $\mathcal{P}^{(l)} = \bigcup_f \mathcal{P}^{(l,f)}$. Define $\mathcal{S}^{(l)} = \mathcal{K}^{(l)} \setminus \mathcal{P}^{(l)}$ as the remaining active tokens. The attention output can be decomposed as:

$$z_q^{(l)} = \underbrace{\sum_{i \in \mathcal{S}^{(l)}} \alpha_{q,i}^{(l)} v_i^{(l)}}_{\text{remaining retained-token contribution}} + \underbrace{\sum_{j \in \mathcal{P}^{(l)}} \alpha_{q,j}^{(l)} v_j^{(l)}}_{\text{event-unsupported peripheral contribution}}. \quad (13)$$

When attention-based pruning preferentially retains tokens in $\mathcal{P}^{(l)}$, these tokens occupy the limited visual-token budget and continue contributing keys and values to later attention computation. Under high compression, each such token also displaces a potentially structure-relevant visual token, weakening the retained visual context.

C.2 Mechanism: Cascading Degradation Across Layers

The degradation can propagate through the network. At pruning layer l , if the retained visual-token set contains many event-unsupported peripheral tokens, their values contribute to the layer output and their representations are forwarded through residual connections and feed-forward blocks. Subsequent attention layers then operate on this biased retained set. If later pruning decisions are again based mainly on attention scores, the same peripheral sink tokens can be repeatedly favored, causing the error to compound.

This mechanism is most harmful at aggressive retention ratios, where the token budget is too small to mask suboptimal token placement. This is consistent with the empirical results in Table 1: attention-based baselines such as FastV and PyramidDrop degrade substantially at 20% retention, whereas ECP maintains robust accuracy by incorporating event-guided calibration.

C.3 Solution: EARF as a Purification Mechanism

EARF mitigates this issue by using event saliency only at the score-and-mask level, without encoding events as additional hidden states. For pruning layer l and keyframe f , EARF uses the text-conditioned attention score $A_i^{(l,f)}$ from the preceding head-averaged post-softmax multimodal self-attention map, following the main-text definition, and the EMSF event saliency $M_i^{(f)}$ for the same visual token. Although attention is computed over the global active sequence, EARF calibrates and ranks visual tokens within each keyframe set $\mathcal{V}^{(l,f)}$, matching the implementation. To avoid scale mismatch, both signals are projected into a shared per-keyframe rank space:

$$R_{\mathcal{V}^{(l,f)}}(\phi, i) = \frac{\text{rank}_{\mathcal{V}^{(l,f)}}(\phi_i)}{\max(|\mathcal{V}^{(l,f)}| - 1, 1)}, \quad \phi \in \{A^{(l,f)}, M^{(f)}\}. \quad (14)$$

The calibrated EARF score is:

$$S_{\text{calib}}^{(l,f,i)} = (1 - \gamma_l)R_{\mathcal{V}^{(l,f)}}(A^{(l,f)}, i) + \gamma_l R_{\mathcal{V}^{(l,f)}}(M^{(f)}, i). \quad (15)$$

Consider an event-unsupported peripheral sink token j with high attention rank but weak event support:

$$R_{\mathcal{V}^{(l,f)}}(A^{(l,f)}, j) \approx 1, \quad R_{\mathcal{V}^{(l,f)}}(M^{(f)}, j) \approx 0.$$

Attention-only pruning would assign this token a near-maximal score. In EARF, however, its calibrated score becomes:

$$S_{\text{calib}}^{(l,f,j)} \approx 1 - \gamma_l. \quad (16)$$

By contrast, an event-supported token u with comparable attention rank and high event rank obtains:

$$S_{\text{calib}}^{(l,f,u)} \approx 1.$$

More generally, the score gap between an event-supported token u and an event-unsupported token j in the same keyframe is:

$$S_{\text{calib}}^{(l,f,u)} - S_{\text{calib}}^{(l,f,j)} = (1 - \gamma_l)\Delta R_A + \gamma_l\Delta R_M, \quad (17)$$

where $\Delta R_A = R_{\mathcal{V}^{(l,f)}}(A^{(l,f)}, u) - R_{\mathcal{V}^{(l,f)}}(A^{(l,f)}, j)$ and $\Delta R_M = R_{\mathcal{V}^{(l,f)}}(M^{(f)}, u) - R_{\mathcal{V}^{(l,f)}}(M^{(f)}, j)$. When the two tokens have comparable attention ranks and their event ranks differ substantially, the margin is dominated by the event term and is approximately γ_l . Importantly, EARF does not simply penalize all peripheral tokens: a peripheral token with strong event support can still be retained. The mechanism specifically targets tokens whose attention rank is inflated but whose event rank is low.

Given the layer-wise retention budget $K_l^{(f)}$, EARF keeps the visual-token set $\mathcal{I}_{\text{EARF}}^{(l,f)}$ with the highest calibrated scores in each keyframe. After per-keyframe pruning, the retained visual tokens are merged across keyframes, yielding:

$$\tilde{\mathcal{V}}^{(l)} = \bigcup_f \mathcal{I}_{\text{EARF}}^{(l,f)}, \quad \tilde{\mathcal{K}}^{(l)} = \mathcal{T}^{(l)} \cup \tilde{\mathcal{V}}^{(l)}. \quad (18)$$

For any pruned visual token $j \notin \tilde{\mathcal{V}}^{(l)}$, its key and value are no longer forwarded to subsequent layers. The attention output is therefore computed over a purified active set:

$$\tilde{z}_q^{(l)} = \sum_{i \in \tilde{\mathcal{K}}^{(l)}} \tilde{\alpha}_{q,i}^{(l)} v_i^{(l)}, \quad \tilde{\alpha}_{q,i}^{(l)} = \frac{\exp\left(q^\top k_i^{(l)} / \sqrt{d_k}\right)}{\sum_{r \in \tilde{\mathcal{K}}^{(l)}} \exp\left(q^\top k_r^{(l)} / \sqrt{d_k}\right)}. \quad (19)$$

This removes event-unsupported position-biased keys and values from downstream attention, increasing the relative proportion of tokens that carry semantic, motion, or geometric support.

C.4 Connection to Attention Sink Literature

Prior work on efficient LLMs identified that certain tokens in autoregressive models can act as ‘‘attention sinks’’, accumulating attention mass regardless of semantic relevance. Our analysis reveals

an analogous spatial phenomenon in vision-language models: peripheral visual tokens can serve as two-dimensional attention sinks due to positional biases.

The key difference is that event streams provide an external motion/structure cue for distinguishing structure-supported tokens from event-unsupported peripheral artifacts. Unlike text-only settings where sink tokens must be detected from internal attention statistics alone, EARF leverages token-aligned event saliency as a training-free prior to calibrate pruning decisions. This external prior reduces the downstream presence of event-unsupported position-biased keys and values while preserving semantic attention through the layer-wise weight γ_l .

D Simulated Event Generation Protocol

For RGB-only public benchmarks, we generate simulated events offline with vid2e from each original source video at its native frame rate. If a video is recorded at 30 fps, vid2e is run on the full 30-fps sequence and synthesizes events between adjacent original frames by triggering events when interpolated logarithmic brightness changes exceed the contrast thresholds. We use the standard setting $c_p = 0.2$, $c_n = 0.2$, and $t_{\text{ref}} = 0$, where c_p and c_n are the positive and negative contrast thresholds and t_{ref} is the refractory period. This offline synthesis is used only to construct paired RGB-event inputs for benchmarks without native events; it is excluded from the reported online inference latency/GFLOPs. For ESR-Real, events are captured directly by the Prophesee EVK4 hardware and do not require vid2e simulation.

E ESR-Real Dataset

To comprehensively evaluate the embodied cognition capabilities of models during motion, we designed a structured benchmark consisting of three primary dimensions: *Perception*, *Cognition*, and *Reasoning & Planning*. Each cognitive ability is manifested through specific sub-tasks. We provided handcrafted question prototypes for each task to ensure the evaluation captures the model’s spatial reasoning rather than linguistic patterns. The task set logic is as follows:

- **Perception:** This level evaluates the model’s foundational ability to recognize environmental goals (Goal Perception) and maintain visual continuity during camera movement (Trajectory Scene).
- **Cognition:** Moving beyond raw vision, these tasks measure the model’s capacity to internalize spatial metrics, such as calculating relative proximity (Relative Distance) and predicting metric changes during dynamic actions (Motion Assumption).
- **Reasoning & Planning:** This is the highest level of embodied intelligence, requiring the model to resolve orientation-based logic (Direction Reasoning) and generate strategic action sequences based on current orientation and target goals (Route Planning).

E.1 Hardware Setup

ESR-Real is captured using a synchronized RGB-event camera rig consisting of two sensors rigidly mounted on a custom handheld platform:

Event Camera: Prophesee EVK4 HD, equipped with the Sony IMX636ES event-based vision sensor. Key specifications include: 1280×720 pixel resolution, $4.86 \mu\text{m}$ pixel pitch, >120 dB dynamic range, microsecond-level temporal resolution (equivalent to $>10,000$ fps), and low-light sensitivity down to 0.08 lux. The asynchronous pixel-level readout enables motion capture without motion blur, making it ideal for first-person dynamic spatial reasoning under ego-motion.

RGB Camera: Hikvision MV-CS050-10UC industrial camera, featuring the Sony IMX264 global shutter CMOS sensor. Specifications: 2448×2048 pixel resolution (5 MP), $3.45 \mu\text{m}$ pixel pitch, up to 60 fps frame rate, and USB 3.0 interface. The global shutter eliminates rolling shutter artifacts, ensuring geometric consistency with the event stream.

Both cameras are rigidly mounted on a 3D-printed bracket with a baseline of approximately 5 cm, enabling synchronized capture of the same scene from nearly co-located viewpoints.

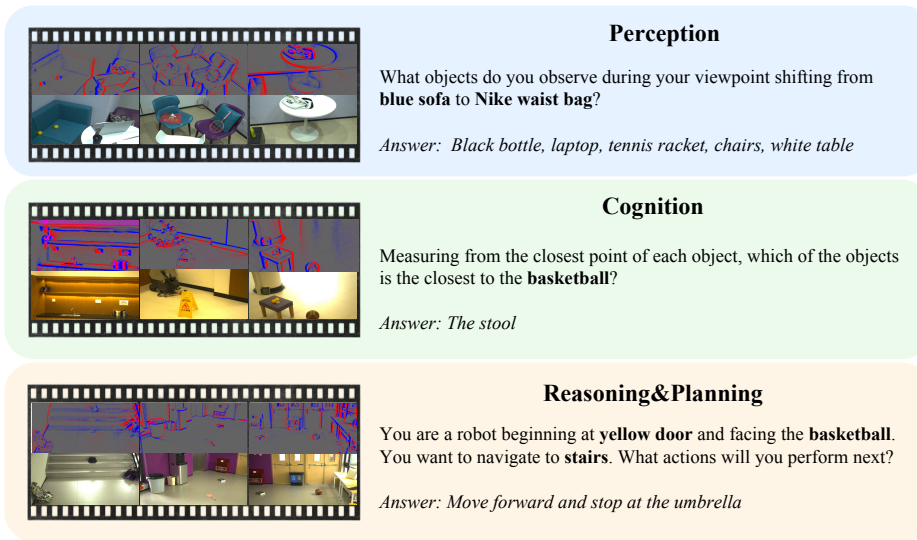


Figure 9: ESR-Real dataset overview

Table 9: ESR-Real task set overview.

Perception	
Goal Perception	At the initial position, you are asked to navigate to the {target_object}. When you reach the last frame of the video, is the destination within view at your current location?
Trajectory Scene	What objects do you observe during your viewpoint shifting along {trajectory_reference}
Cognition	
Relative Distance	Measuring from the closest point of each object, which of these objects is the closest to the {target_object}?
Motion Assumption	How does the distance between you and the {target_object} change during your {action_description}?
Reasoning & Planning	
Direction Reasoning	You're a robot standing by the center of {position_object} and facing the center of {orient_object}, is the center of {query_object} to my left, right, or back? (Back defined as ≥ 135 degrees turn)
Route Planning	You are a robot beginning at {position_object} and facing the {orient_object}. You want to navigate to {end_object}. What actions will you perform next?

E.2 Stereo Calibration and Alignment

To project RGB frames and event streams into a common coordinate system, we perform stereo calibration. The calibration procedure consists of three stages:

Camera Calibration: We employ Zhang’s flexible calibration method [45] for both intrinsic and extrinsic parameter estimation. For the RGB camera, we capture 20–30 images of a 4×7 checkerboard pattern (square size: 80 mm) at various orientations and distances. Corner detection is performed using sub-pixel refinement, and the camera parameters are estimated via nonlinear optimization. For the event camera, we use Prophesee’s Metavision SDK calibration pipeline with a blinking checkerboard pattern displayed on a monitor. The blinking pattern generates consistent events at pattern boundaries, enabling reliable corner detection directly from the event stream.

Stereo Calibration: To estimate the extrinsic parameters between the RGB and event cameras, both sensors simultaneously capture the same 4×7 checkerboard pattern. Since event cameras output asynchronous event streams rather than intensity images, we first reconstruct intensity frames from the event stream using E2VID [29]. Using the detected corners from both the RGB frames and E2VID-reconstructed event frames, we estimate the rotation matrix \mathbf{R} and translation vector \mathbf{t} that define the rigid transformation between the two camera coordinate systems.

Event-RGB Alignment: Using the calibrated stereo parameters, we warp RGB frames into the event camera’s coordinate system. Event streams remain in their native resolution (1280×720 pixels), while RGB frames are projected onto the event image plane to achieve pixel-level alignment.

E.3 Data Collection Protocol

Data collection was conducted across diverse indoor environments including offices, laboratories, corridors, and common areas. Each recording session involves handheld traversal with natural ego-motion (walking, turning, approaching objects), with sequence durations ranging from 50 to 100 seconds. RGB video and continuous event streams are recorded simultaneously, followed by post-capture annotation of spatial reasoning QA pairs by the internal research team.

The final ESR-Real benchmark comprises over 700 QA pairs across 6 task categories, covering perception, cognition, and reasoning capabilities essential for embodied AI systems.

E.4 MCQ Generation

This section details our automated annotation pipeline, designed to scale the production of high-quality spatial reasoning benchmarks. The objective is to leverage the robust visual perception and logical reasoning capabilities of advanced Large Multimodal Models (LMMs) to transform raw egocentric videos into structured, logic-grounded datasets.

We have designed a multi-stage Chain-of-Thought (CoT) framework tailored for embodied spatial understanding, consisting of the following two primary stages:

Stage 1: Translating visual information into a comprehensive topological and spatial metadata map.

Object Segmentation and Disambiguation: The model identifies the 20 most salient and identifiable objects within the video. To prevent ambiguity, a strict “Unique Naming” protocol is enforced. If multiple objects of the same category exist (e.g., two monitors), they are assigned unique identifiers based on objective visual attributes (e.g., “monitor by the window”) while avoiding unquantifiable subjective adjectives (e.g., “nice”, “big”).

Fine-grained Spatial Mapping: The system generates over 25 detailed spatial descriptions covering relative orientations, distances, and overall scene layout.

Proximity Identification: All object pairs within a 1-meter radius are explicitly mapped as “proximity pairs” to serve as constraints for subsequent logic generation.

Stage 2: Logic-driven QA Synthesis—Populate complex reasoning templates with the structured metadata.

Spatial Reasoning Logic Constraints: To ensure that questions require high-level reasoning rather than simple local associations, we implement a “Non-Proximity Constraint.” For instance, objects selected for Route Planning and Scene Recall must not be proximity pairs, forcing the model to reason over extended trajectories.

Automated Template Population: The system systematically varies reference frames (robot position and orientation) to generate diverse perspectives. Rigorous filters are applied to ensure that the correct options (ground truth) are derived directly from the Stage 1 metadata and that distractors are logically distinct.

By utilizing Gemini-3Pro at this stage, we ensure that the generated questions are grounded in a deep understanding of the 3D environment, providing a challenging and high-fidelity benchmark for embodied AI agents.

E.5 Manual QA Refinement

The generated MCQs may contain invalid questions, ambiguous options, incorrect answers, and various other issues that require further manual QA refinement. These issues stem from two main sources: a) Even the most advanced Video-LLMs lack the ability to fully understand fine-grained embodied movements within confined indoor spaces. b) The indoor scenarios are densely populated and spatially complex, making dynamic video comprehension challenging. We approach the manual QA refinement process from four aspects:

- a) **Invalid/ambiguous questions:** For example, in Goal Perception tasks, an instruction to “navigate to the chair” leads to ambiguity when multiple chairs are present in a living room. The navigation target should be clarified to “navigate to the wooden armchair near the window” to ensure precise target identification.
- b) **Object hallucination:** This refers to the presence of furniture or indoor elements in the correct option that were never actually captured during the Trajectory Scene (e.g., mentioning a lamp that was occluded or absent).
- c) **Spatial and metric inaccuracies:** Descriptions involving Direction Reasoning or Relative Distance are often incorrect or imprecise due to the constantly changing camera perspective during motion.
- d) **Choices with insufficient differentiation or logic errors:** In Motion Assumption and Route Planning tasks, one scenario is that distractors are too similar to the correct action sequence. Another is that the ground truth failed to represent the optimal strategic action based on the agent’s current orientation.

The entire refinement process required over 200 person-hours.

F Remaining Results of Effectiveness Experiment

In the main text, we report six representative task columns from UrbanVideo-Bench and VSI-Bench due to space. This appendix reports the remaining seven task columns; together with Table 1, the results cover all 13 selected tasks used to compute Avg.Acc. Table 10 shows that ECP is particularly stable under aggressive compression. When the retention rate drops to 20%, VTW decreases to 30.50%, whereas ECP maintains 37.62%, close to its 70% retention result. This trend suggests that event-assisted pruning helps preserve motion- and geometry-relevant evidence when the token budget becomes sparse. The remaining task columns show the following patterns:

- a) **Perception:** ECP remains strong on Object Recall and Scene Recall. At 20% retention, it achieves 73.68% in Object Recall, higher than the full-token baseline’s 65.79%, suggesting that the retained tokens can still cover key environmental entities.
- b) **Cognition:** ECP maintains the highest Cognitive Map accuracy of 54.36% at 20% retention, indicating stronger layout consistency under sparse token budgets.
- c) **Reasoning & Planning:** For High-Level Planning, ECP is consistently strong across pruning ratios, achieving 50.00% accuracy at 70% retention and 52.12% at 20% retention. At 70% retention, it clearly outperforms BTP (44.49%) and DivPrune (42.80%), while other baselines show larger variation across retention ratios.

G Additional Ablation Study of Component Analysis

To provide a more granular view of each component, we conduct an ablation study on the combined validation set of UrbanVideo-Bench and VSI-Bench. We analyze Event-Triggered Causal Sampling (ETCS), Event-guided Motion Saliency Filtering (EMSF), and Event-Attention Ranking Fusion (EARF) under token retention rates of 20%, 50%, and 70%, and report averaged accuracy. The results are summarized in Table 11.

G.1 Component-wise Contribution Analysis

ETCS: The Spatiotemporal Anchor for Cognition. Our results empirically validate ETCS as the cornerstone of spatial cognition. As shown in Table 11, configurations utilizing ETCS achieve the

Table 10: Accuracy comparison of remaining tasks on first-person dynamic spatial reasoning benchmarks. *Task definitions: **Obj.Recall**=Object Recall, **Scene.Recall**=Scene Recall, **Abs.Dis**=Absolute Distance Estimation; **Cog.Map**=Cognitive Map Construction; **Rel.Dir**=Relative Direction Understanding; **Route.Plan**=Route Planning; **HL.Plan**=High-Level Planning.*

Method	Avg.Acc	Perception		Cognition		Reasoning & Planning		
		Obj.Recall	Scene.Recall	Abs.Dis	Cog.Map	Rel.Dir	Route.Plan	HL.Plan
Original	36.31	65.79	69.70	23.05	51.43	34.74	29.53	45.23
<i>70% Retaining</i>								
BTP	35.95	65.79	69.70	23.31	51.45	34.14	28.19	44.49
DivPrune	36.16	65.79	69.70	23.53	52.28	35.14	30.87	42.80
FastV	36.28	65.79	69.70	23.47	51.87	34.54	28.86	44.49
PDrop	36.73	65.79	69.70	23.85	53.53	35.54	30.87	44.49
DTD	36.36	63.16	69.70	24.01	51.45	35.74	29.53	46.61
VTW	36.45	65.79	69.70	23.97	51.45	35.14	30.20	42.80
DEP	36.88	68.40	69.70	24.28	53.50	36.55	28.90	41.50
OURS	37.78	65.79	69.70	24.32	52.70	33.94	31.54	50.00
<i>50% Retaining</i>								
BTP	35.09	65.79	69.70	22.20	49.38	34.14	30.20	43.64
DivPrune	36.77	63.16	69.70	24.05	53.53	36.14	29.53	46.61
FastV	35.67	65.79	66.67	22.14	50.21	34.74	30.20	47.46
PDrop	35.67	65.79	69.70	22.16	50.62	34.74	28.86	45.76
DTD	36.55	63.16	69.70	24.17	53.11	35.14	29.53	47.03
VTW	33.84	68.42	72.73	22.44	49.38	34.74	30.87	38.98
DEP	33.28	71.10	72.70	21.18	49.00	35.14	30.20	36.50
OURS	38.16	63.16	69.70	24.50	54.36	34.14	32.21	48.73
<i>20% Retaining</i>								
BTP	33.34	65.79	66.67	19.95	51.87	34.74	30.20	47.88
DivPrune	34.40	60.53	66.67	20.33	49.79	35.74	27.52	51.27
FastV	32.64	57.89	63.64	22.79	47.72	32.73	34.23	49.58
PDrop	33.12	63.16	66.67	21.50	53.53	32.53	31.54	48.31
DTD	35.37	65.79	72.73	22.58	52.28	33.53	29.53	47.88
VTW	30.50	42.11	54.55	12.14	47.72	35.54	30.20	41.95
DEP	29.95	42.10	51.50	11.11	44.10	37.35	30.90	42.30
OURS	37.62	73.68	72.73	23.05	54.36	36.95	30.20	52.12

highest accuracy in Cognition tasks (44.7%). Comparing ETCS only with EARF only, the inclusion of ETCS yields a significant gain in Cognition (+1.72%). Without the temporal causality provided by ETCS, downstream reasoning modules operate on misaligned frames, leading to systemic failures in dynamic scene understanding (e.g., mapping and distance estimation).

EMSF: The High-SNR Filter for Reasoning. Unexpectedly, Event-guided Motion Saliency Filtering (EMSF) emerges as the critical driver for logical reasoning. EMSF only achieves the highest performance in Reasoning & Planning (28.31%), slightly outperforming even the Full Model. This suggests that EMSF acts as an aggressive denoising mechanism. By filtering out static background redundancies, it maximizes the Signal-to-Noise Ratio (SNR) for dynamic interactions, allowing the LLM to focus purely on causal motion. However, relying solely on EMSF compromises Cognition (43.11%) due to the loss of background context.

EARF: The Semantic Booster for Perception. Event-Attention Ranking Fusion (EARF) is pivotal for fine-grained visual recognition. Its primary contribution lies in enhancing Perception accuracy. The Full Model (incorporating EARF) achieves the peak Perception score of 50.74%. Comparing ETCS+EMSF to (Full), the addition of EARF provides a clear boost in perception reliability (+0.90%), demonstrating that rank-based fusion effectively harmonizes the high temporal resolution of events with the semantic richness of RGB frames.

G.2 Synergy and Holistic Superiority of the Full Framework

While individual modules show strengths in specific sub-domains—ETCS in Cognition and EMSF in Reasoning—Table 11 shows that Full ECP provides the best overall trade-off, with the highest averaged accuracy (37.85%) and the lowest latency (1.16s) among the tested variants.

Why the Full Model is Optimal. Despite the specialized strengths of single-module baselines, the Full Model demonstrates superior holistic robustness:

Table 11: **Additional ablation study of component analysis.** We perform a granular breakdown of accuracy metrics mapped to the validation baseline. The best results are **bolded** and second-best are underlined. Full ECP achieves the highest overall accuracy and Perception score while maintaining the lowest latency among multi-component variants.

Variant	Components			Latency (s) ↓	Overall Acc (%) ↑	Task Categories Acc (%)		
	ETCS	EMSF	EARF			Perception	Cognition	R&P
ETCS	✓	-	-	1.58	36.52	48.06	44.71	26.67
EMSF	-	✓	-	1.83	37.22	49.20	43.11	28.31
EARF	-	-	✓	1.53	37.15	50.25	42.99	28.18
ETCS+EMSF	✓	✓	-	1.47	37.51	49.84	44.65	27.76
ETCS+EARF	✓	-	✓	1.17	<u>37.75</u>	<u>50.71</u>	<u>44.25</u>	28.01
EMSF+EARF	-	✓	✓	1.59	37.00	48.66	43.68	27.93
Full ECP (Ours)	✓	✓	✓	1.16	37.85	50.74	44.06	<u>28.17</u>

- **Global Maxima:** The Full Model achieves the highest overall accuracy (37.8%) across all configurations. It effectively harmonizes the aggressive spatial filtering of EMSF with the semantic preservation of EARF.
- **Optimal Pareto Frontier:** While EMSF alone achieves the highest Reasoning score (28.31%), it suffers in Cognition and Perception. The Full Model accepts a negligible drop in Reasoning (-0.14%) to achieve a gain in Perception (+1.54%) and Cognition (+0.95%). This trade-off is essential for embodied agents that must simultaneously recognize objects and plan actions.
- **Synergistic Stability:** The Full Model mitigates the high variance observed in partial configurations. For instance, while ETCS + EARF excels in Perception, it lags behind EMSF in Reasoning accuracy. By integrating all three priors, our framework offers the most balanced and generalizable performance for diverse real-world challenges.

H Broader Impacts and Responsible Release

Broader impacts and responsible use. ECP reduces the visual-token computation required by Video-LLMs for first-person spatial reasoning, which may lower latency, memory usage, and energy consumption on resource-constrained RGB-event platforms. These efficiency gains may also support more local processing and reduce reliance on cloud offloading. However, as with other egocentric perception technologies, easier deployment in privacy-sensitive environments could raise monitoring or privacy concerns, and incorrect spatial predictions could affect downstream navigation or interaction decisions. ECP should therefore be treated as an efficiency mechanism for perception rather than a complete decision-making system, and safety-relevant deployment requires task-specific validation, privacy-preserving data handling, human oversight, and compliance with applicable regulations.

Responsible release of ESR-Real. ESR-Real is collected in controlled indoor environments for spatial-reasoning evaluation, not identity recognition. Before release, we review the RGB-event data, QA annotations, and metadata to remove or blur incidental faces, personal identifiers, sensitive documents or screens, and location-revealing metadata when present. The released benchmark will not include identity, biometric, or person-tracking labels, and will be distributed with documentation and research-use terms restricting re-identification, privacy-invasive monitoring, and unvalidated safety-critical deployment.